ChemPubSoc Europe

DOI: 10.1002/cctc.201701680

CHEMCATCHEM Full Papers

Phosphorus-Doped MoS_2 Nanosheets Supported on Carbon Cloths as Efficient Hydrogen-Generation Electrocatalysts

Luozhen Bian[+],[a, b] Wei Gao[+],[c, d] Jiamin Sun,[a, b] Mingming Han,[a, b] Fulin Li,[a, b] Zhaofeng Gao,[a, b] Lei Shu,[d, e] Ning Han,[f] Zai-xing Yang,*[a, b] Aimin Song,[b] Yongquan Qu,*[c] and Johnny C. Ho*[d, e]

Highly efficient and stable non-noble metal electrocatalysts for hydrogen generation are desired for sustainable development of energy conversion and storage. Here, a facile low-temperature phosphidation process is developed for phosphorus doping into molybdenum disulfide (MoS_2) nanosheets directly synthesized on carbon cloths to function as an integrated electrode for efficient hydrogen evolution reaction. The optimal phosphorus-doped (3.3 at%) MoS_2 nanosheets exhibit substantially lower overpotentials of 133 and 189 mV to drive the current densities of 20 and 100 mA cm^{-2}, respectively, as compared with undoped MoS_2, and an impressively small Tafel slope of 67.0 mV dec^{-1}. The excellent stability in acid media also makes the phosphorus-doped MoS_2 nanosheet catalysts promising candidates for hydrogen generation in practical applications.

Introduction

In the past decades, hydrogen has not only been considered as one of the most promising future clean fuels, but also regarded as an ideal carrier to store electricity generated from other renewable energy sources on a large scale for practical applications.[1–3] Particularly, water electrolysis is a simple and ecofriendly approach to simultaneously generate hydrogen and oxygen in acidic, alkaline or neutral media.[4] The efficiency of these hydrogen and oxygen evolutions is closely related to the selection of electrode materials, and hence, it is important to develop low-cost, highly active and stable electrocatalysts for sustainable water splitting. At the same time, although Pt is known to be a very electrocatalytically active and stable material for hydrogen evolution reaction (HER), its high cost and scarcity greatly restrict its industrial utilizations.[5,6] In this regard, extensive efforts have been devoted to investigate highly efficient, non-noble metal electrocatalyst materials with low overpotentials and large HER current densities. Among many promising recent candidate materials, owing to the large capacities of well-known catalytically active edge sites and excellent stability, two-dimensional (2D) transition-metal dichalcogenides (TMDs), such as molybdenum disulfide (MoS_2) nanosheets, have attracted substantial attention for making electrochemical hydrogen production efficient.[7–10]

Previously, MoS_2 was researched as a potential candidate for HER because of its low free energy of hydrogen adsorption, as demonstrated by theoretical and experimental analyses.[11] Nevertheless, the bulk MoS_2 crystal usually performs as a poor HER electrocatalyst because of its relatively low content of active catalytic sites and small specific surface area. In this case, many methods have been employed to enhance the quantity of electrochemically active sites and enlarge the surface area. For example, defect engineering is a newly developed method to reconstruct the surface of MoS_2 with more edges and defects, which helps to expose more active catalytic

[a] L. Bian,[+] J. Sun, M. Han, F. Li, Z. Gao, Prof. Z.-x. Yang
Shenzhen Research Institute
Shandong University
Shenzhen, 518057 (P.R. China)
E-mail: zaixyang@sdu.edu.cn

[b] L. Bian,[+] J. Sun, M. Han, F. Li, Z. Gao, Prof. Z.-x. Yang, Prof. A. M. Song
Center of Nanoelectronics and School of Microelectronics
Shandong University
Jinan, 250100 (P.R. China)

[c] W. Gao,[+] Prof. Y. Q. Qu
Center for Applied Chemical Research,
Frontier Institute of Science and Technology
Xi'an Jiaotong University
Xi'an, 710049 (P.R. China)
E-mail: yongquan@mail.xjtu.edu.cn

[d] W. Gao,[+] L. Shu, Prof. J. C. Ho
Department of Materials Science and Engineering
City University of Hong Kong
83 Tat Chee Avenue, Kowloon, Hong Kong (P.R. China)
E-mail: johnnyho@cityu.edu.hk

[e] L. Shu, Prof. J. C. Ho
Shenzhen Research Institute
City University of Hong Kong
Shenzhen, 518057 (P.R. China)

[f] Prof. N. Han
State Key Laboratory of Multiphase Complex Systems
Institute of Process Engineering, Chinese Academy of Sciences
Beijing, 100190 (P.R. China)

[+] These authors contributed equally to this work.

Supporting information and the ORCID identification number(s) for the author(s) of this article can be found under: https://doi.org/10.1002/cctc.201701680.

sites of unsaturated sulfur atoms.[12–14] On the other hand, controllable disorder engineering has also been demonstrated in oxygen-incorporated MoS_2 ultrathin nanosheets for efficient hydrogen evolution.[13] Furthermore, interface engineering on the surface of nanostructured MoS_2 by building a heterogeneous catalyst is also well established to increase the number of surface active sites and, correspondingly, to improve the catalytic properties.[15–17] Recently, doping engineering has also been proved as a very effective technique to create active catalytic sites on MoS_2 nanosheets. Owing to their earth abundance and good stability,[18–20] several dopants, such as phosphorus, carbon, and nitrogen, are widely employed as dopants in MoS_2 nanosheets to lower the energy barrier of the water-dissociation step and to facilitate the desorption of the as-formed hydroxide species to accelerate HER processes.[12,13,21] Specifically, Liu et al. have reported that P dopants in the MoS_2 matrix can significantly enhance the HER activity not only by increasing the quantity of intrinsic basal-plane active sites, but also by enhancing the conductivity of the materials.[22] Moreover, it would be extremely attractive to prepare an integrated electrode of phosphorus-doped MoS_2 on a flexible substrate to afford the large current density for practical utilizations.

In this work, we demonstrate the successful synthesis of P-doped MoS_2 nanosheets on carbon cloths (CC) directly as an integrated electrode and then investigate the effect of phosphorus doping for the corresponding HER processes. The relationship between doping conditions and electrochemical catalytic properties is also investigated to achieve high-performance catalysts based on MoS_2 nanosheets with optimal P doping. Importantly, after optimized gas-phase phosphidation, the obtained catalysts preserve their initial nanosheet morphology but present an apparent improvement in their catalytic activity with a low overpotential of 133 mV to drive the current density of 20 mA cm^{-2}, along with the excellent electrochemical stability. All these results revealed the technological potency of our P-doped MoS_2 nanosheets on CC as an integrated electrode for highly efficient hydrogen evolution.

Results and Discussion

MoS_2 nanosheets directly supported on carbon cloths were prepared through a simple hydrothermal method, and their morphologies were studied by SEM. As shown in Figure 1a, the sheet-like morphology of MoS_2 is revealed with the size of hundreds of nanometers, with the inset image exhibiting uniform distribution of the nanosheets on carbon cloths. Doping phosphorous element is then realized by using a low-temperature gas-phase phosphidation method, by which $NaH_2PO_2{\cdot}H_2O$ is used as the phosphorous evaporation source with various time duration intervals (namely, 30, 60, and 90 min). Previously, Tour et al. reported the formation of mixed phases of $MoS_{2(1-x)}P_x$ with enhanced catalytic properties for HER by thermally annealing mixtures of MoS_2 and red phosphorus at up to 1023 K, but the nanosheet dimension and morphology were inevitably altered.[23] In contrast, in this work, an inorganic salt of $NaH_2PO_2{\cdot}H_2O$ was employed as the phosphorous source to dope MoS_2 nanosheets at a much lower temperature of 573 K,

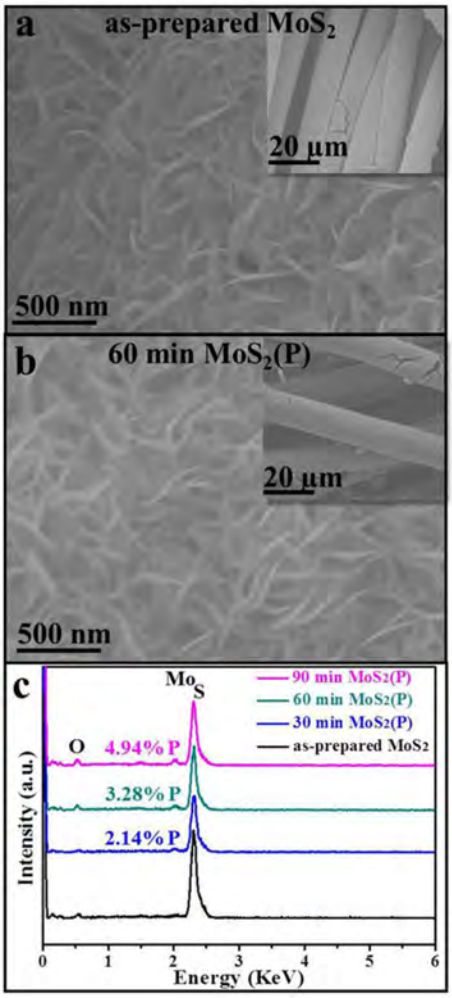

Figure 1. Morphology and composition of the as-prepared MoS_2 nanosheets and P-doped MoS_2 nanosheets directly synthesized on carbon cloths. (a, b) SEM images of MoS_2 nanosheets and P-doped MoS_2 nanosheets, (c) EDS spectra of MoS_2 nanosheets and P-doped MoS_2 nanosheets.

resulting in the preservation of the nanosheet morphology. As displayed in Figure 1b and Supporting Information Figure S1a–d, the morphologies of all P-doped MoS_2 nanosheets supported on CC and processed at different doping duration (i.e., 30, 60, and 90 min) are well preserved as compared to the as-prepared undoped MoS_2 nanosheets (Figure 1a). In addition, energy dispersive X-ray spectroscopy (EDS) further confirms the existence of P dopants in MoS_2 nanosheets (Figure 1c). Clearly, the P-doped MoS_2 nanosheets show a higher P doping content with longer P doping duration. Specifically, the doping concentration was determined to be 2.1, 3.3, and 4.9 at.% for the samples processed for 30, 60, and 90 min of P doping, respectively. At the same time, small peaks of oxygen with an energy of ≈0.55 keV are observed in the EDS spectra of all samples. The oxygen element may come from the adsorbed water molecules and surface hydroxide species upon air exposure, even after calcining in Ar. For the P-doped MoS_2 samples, partial oxidation of phosphorus can also lead to the existence of oxygen. The crystal structure and phase of the as-prepared samples were then studied by X-ray diffractometry

(XRD). The corresponding XRD pattern exhibits the hexagonal structure of MoS_2, which perfectly agrees with the crystal phase of 1T-molybdenite of MoS_2 (Figure S1 e).[24] Also, broad peaks at approximately 26° and 43° can be ascribed to the carbon cloth as reported in the literature.[25,26] More importantly, the thorough XRD characterization indicates that all P-doped MoS_2 samples have the crystalline structure of 2H-MoS_2 (PDF# 37-1492),[23,24] which is uniquely different from that of the undoped MoS_2/CC sample. This conversion of crystalline structure from 1T to 2H phase is mainly related to the poor thermal stability of 1T-MoS_2 as well as the rapid transformation to the thermodynamically stable 2H phase occurring during the low-temperature phosphidation process.[24] All these findings demonstrate that our low-temperature P doping in MoS_2 nanosheets can preserve the sheet morphology and lead to the effective phase transformation from 1T to 2H crystalline structures.

To shed light on the composition and microstructure of the as-prepared MoS_2 nanosheets and P-doped MoS_2 nanosheets, high-resolution transmission electron microscopy (HRTEM) and elemental mapping characterizations were performed. As depicted in Figure 2 a,b insets, MoS_2 nanosheets with the size of hundreds of nanometers are both observed for the undoped and P-doped samples, which is perfectly consistent with the SEM results (Figure 1 a,b). In addition, the HRTEM images exhibit clear and distinct interplanar spacings of 0.31 and 0.29 nm, corresponding to the (1 1 1) and (1 0 0) planes of undoped 1T-MoS_2, respectively (Figure 2 a),[27] and yield the interplanar spacings of 0.25 and 0.22 nm, attributable to the (0 0 5) and (1 0 3) planes of P-doped 2H-MoS_2, respectively (Figure 2 b). The results again confirm the phase transformation of MoS_2 nanosheets from 1T to 2H structure induced by the P doping as observed in the XRD patterns.

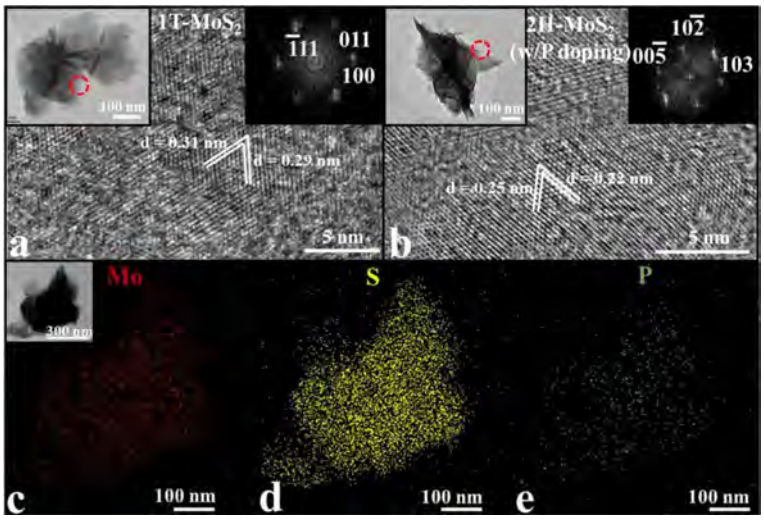

Figure 2. Electron microscopy characterization of as-prepared MoS_2 nanosheets and P-doped MoS_2 nanosheets. (a, b) HRTEM images and the corresponding fast Fourier transform (FFT) of the representative MoS_2 nanosheet and P-doped MoS_2 nanosheet (3.3 at%), respectively. The insets show the low-resolution TEM images of the samples. Red circles indicate the region for the high-resolution imaging given in the main panels. (c, d, e) Scanning TEM image (inset) and corresponding EDS mapping of the P-doped MoS_2 nanosheet (3.3 at%), indicating the uniform distribution of Mo, S and P.

Furthermore, more crystal defects are qualitatively seen in P-doped MoS_2 nanosheets than in the undoped ones (Figure 2 b). These additional crystal defects can be accredited to the elemental substitution of P into S sites in MoS_2 microstructures.[28] Notably, based on the EDS mapping (Figure 2 c–e), all constituents, including the P dopants, are uniformly distributed, indicating that the P atoms are successfully and homogeneously doped into MoS_2 without deteriorating the nanosheet morphology.

Apart from morphology, crystallinity, and composition, it is also important to assess the surface chemical states of all MoS_2 samples. X-ray photoelectron spectroscopy (XPS) was utilized to characterize any change in the surface chemical state before and after P doping in the MoS_2 nanosheets. As depicted in the P 2p spectra in Figure 3 a, no peaks are observed for the undoped MoS_2 sample, whereas a peak is found at 133.4 eV for all P-doped MoS_2 samples. This peak is believed to result from the surface oxidized phosphate species if P atoms are doped into the lattice of MoS_2.[29,30] On the other hand, for the Mo 3d and S 2p spectra as shown in Figure 3 b,c, a tiny peak at 225.6 eV as well as strong peaks at 228.3 eV and 231.5 eV are visible, corresponding to the Mo–S bond, and Mo^{4+} species of Mo $3d_{5/2}$ and Mo $3d_{3/2}$,[17] and another set of strong peaks at 161.2 eV and 162.3 eV for $2p_{3/2}$ and $2p_{1/2}$ orbitals of S^{2-} species in undoped MoS_2, respectively.[13,28] After P doping, the spectra of Mo 3d and S 2p of MoS_2 are still similar to those of the undoped one, except for the apparent shifts in their binding energies. Explicitly, the peaks of Mo 3d spectra are shifted to 226.0, 228.9, and 232.0 eV, correspondingly; and for the S 2p spectra, the peaks are moved to 161.7 eV and 162.9 eV, respectively. These peak shifts may be related to the low-temperature annealing process, indicating that elemental substitution of P into S sites occurred in MoS_2 crystals during the doping process. The similar peak-shift phenomenon has also been witnessed in a previous literature, in which the shifts in binding energies for substitutional doped MoS_2 was revealed.[17] At the same time, this occurrence also suggests that annealing at 673 K may lead to phase transition from 1T-MoS_2 to 2H-MoS_2, accompanied with a downshift of the binding energy of Mo as demonstrated by Xiang et al.[31] Therefore, the changes observed for the surface chemical states of P-doped MoS_2 as compared with those of the undoped MoS_2 have evidently demonstrated the interaction of P dopants and MoS_2 as a result of the low-temperature phosphidation process.

Besides, catalytic activity as well as durability of the electrocatalysts of various P-doped MoS_2 and undoped MoS_2 nanosheets were evaluated in acidic H_2SO_4 (0.5 M, pH 0.6) electrolyte using a three-electrode system. Polarization curves of all catalysts were measured by using the linear sweeping voltammetry (LSV) method at a scan rate of 5 mV s^{-1}. As shown in Figure 4 a, to obtain a HER catalytic current density of 20 mA cm^{-2}, an overpotential of 170 mV is required for undoped MoS_2, and an additional overpotential of 200 mV is needed for simply annealed

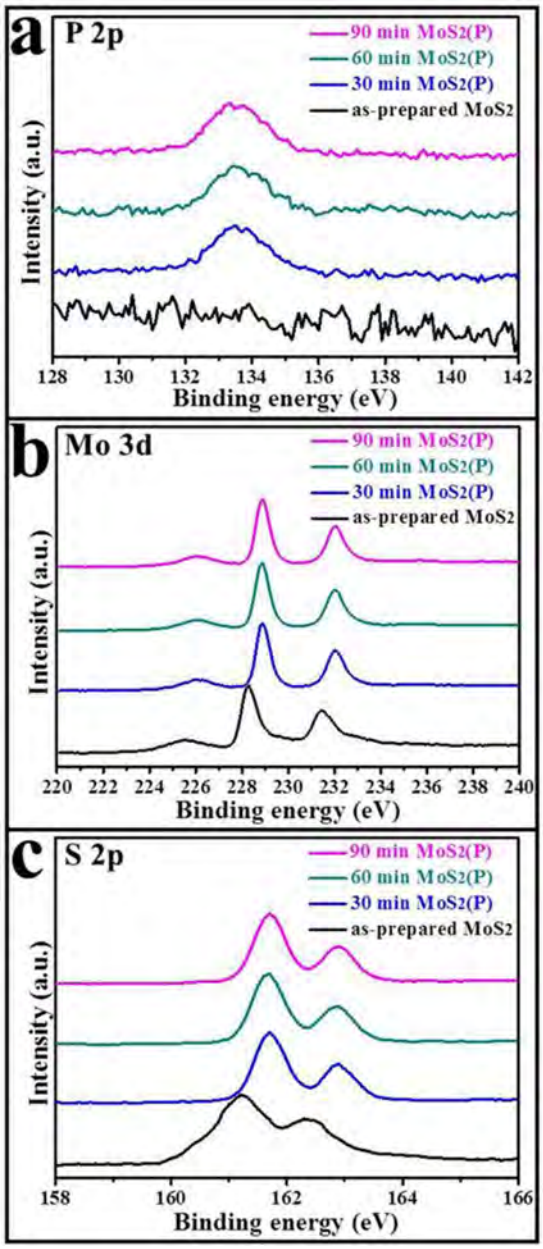

Figure 3. Surface elemental analysis of as-prepared MoS_2 nanosheets and P-doped MoS_2 nanosheets. (a) P 2p bonding region, (b) Mo 3d bonding region, (c) S 2p bonding region.

MoS_2 (60 min) in Ar, which served as the control sample without any P doping for the consistent study here. Based on the XRD results (Figure S1 e), crystalline phase transformation of MoS_2 from 1T to 2H structures proceeds during the low-temperature phosphidation process. As the metallic 1T phase of the MoS_2 nanosheets was demonstrated to have better electrocatalytic performance than the semiconductor 2H phase sample owing to electrochemical oxidation of the edges of 2H phase nanosheets leading to a dramatic reduction in their catalytic activities,[32,33] this phase transformation perfectly explains the degradation in overpotential of the annealed control sample. However, if the P doping is performed along with the annealing process, the overpotentials of all P-doped MoS_2 nanosheet samples are reduced significantly to 156, 133, and 152 mV for the doping (i.e., annealing) duration of 30 (2.1 at.%), 60 (3.3 at%), and 90 min (4.9 at%), respectively, compared to the overpotential of the undoped sample of 170 mV to reach the same current density of 20 mA cm^{-2}. Even for the higher current density of 100 mA cm^{-2}, a similar trend is observed with the overpotential values of 257, 227, 189, and 217 mV for the undoped sample and the 2.1, 3.3, and 4.9 at.% P-doped MoS_2 nanosheet samples, correspondingly. Among all the catalysts, 3.3 at.% P-doped MoS_2 nanosheets (i.e., 60 min doping duration) exhibit the best electrochemical activity, although they consist of the semiconductor 2H phase, instead of the metallic 1T phase.

To evaluate their kinetic properties, Tafel equation was employed to describe the relationship between current and overpotential:

$$\eta = b \log (j/j_0)$$

in which η is the overpotential (mV), b is the Tafel slope (mV dec^{-1}), j is the current density (mA cm^{-2}), and j_0 is the exchange current density (mA cm^{-2}).[34] As extracted from Figure 4 a, after *iR* correction, the Tafel slope of 3.3 at.% P-doped MoS_2 (60 min doping duration) is found to be 67.0 mV dec^{-1}, which is smaller than the ones of the 2.1 at.% P-doped nanosheets (77.6 mV dec^{-1}), 4.9 at.% P-doped nanosheets (71.1 mV dec^{-1}), undoped nanosheets (102.9 mV dec^{-1}), and the annealed control sample (138.9 mV dec^{-1}). Based on the Tafel slope without *iR* correction (shown in Figure S2), MoS_2 nanosheets treated with an optimal P doping of 60 min also show the superior electrochemical HER activity. Clearly, an optimal P doping (i.e., 3.3 at.%) is needed to enhance the number of active catalytic sites and to improve the conductivity and, thus, to achieve superior electrochemical HER activity of MoS_2 nanosheets directly synthesized on carbon cloths as an integrated electrode system. As shown in Supporting Information Table S1, by using the adopted simple low-temperature annealing process, the HER performance of as-prepared P-MoS_2 nanosheets on CC is comparable or even better than others reported in the literature.[13,17,35–37] To further study the difference in their intrinsic properties, the electrochemical active surface area (ECSA) established from the electrochemical double-layer capacitance of the catalyst surface was as well utilized to compare the difference in catalytic active sites.[38] As ECSA is proportional to the electrochemical double-layer capacitance (C_{dl}) in the non-Faradaic potential region, herein, cyclic voltammogram (CV) curves with various scan rates were measured to calculate the C_{dl} values. CV curves of undoped MoS_2 and P-doped (3.3 at.%) MoS_2 nanosheets were then scanned with rates of 10, 20, 30, 40, and 50 mV s^{-1} and complied in Figure S3. The extracted C_{dl} values of undoped MoS_2 and P-doped (3.3 at.%) MoS_2 samples are found to be 7.0 and 17.6 mF cm^{-2}, respectively (Figure 4 c), illustrating that the P doping can indeed result in more active sites for more efficient catalytic hydrogen generation. Furthermore, the catalytic activity normalized to ECSA is also given in Figure S4, suggesting the better intrinsic

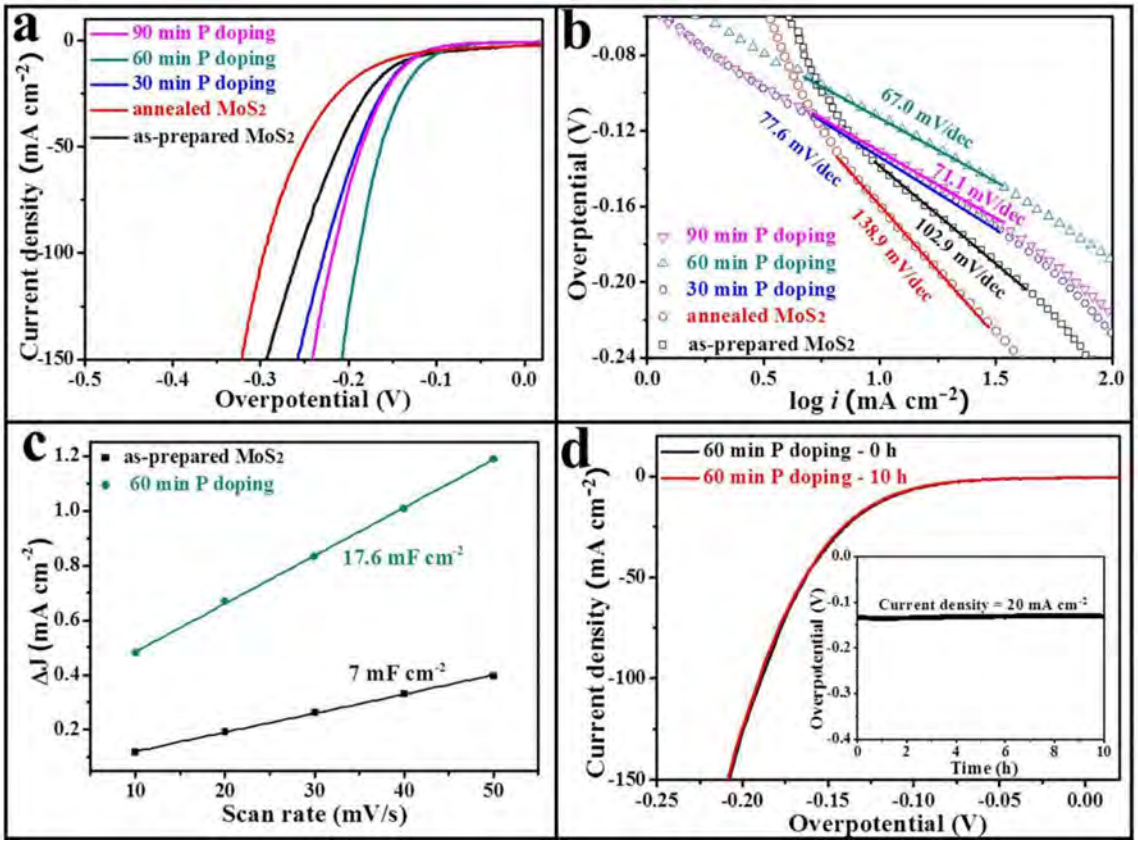

Figure 4. Electrochemical properties of both MoS_2 nanosheets and P-doped MoS_2 nanosheets. (a) Polarization curves of as-synthesized MoS_2 nanosheets, P-doped MoS_2 nanosheets with various doping durations (30, 60, and 90 min), and simply annealed MoS_2 nanosheets; all measurements are performed in 0.5 M H_2SO_4 solution; (b) Tafel slopes derived from (a); (c) plot of capacitive current densities as a function of scan rates for as-synthesized MoS_2 nanosheets and P-doped MoS_2 nanosheets at a doping duration of 60 min; (d) polarization curves of P-doped MoS_2 nanosheets at a doping duration of 60 min before and after the stability tests. The inset shows the stability test of P-doped MoS_2 nanosheets at a doping duration of 60 min and a fixed current density of 20 mA cm^{-2}.

activity of P-doped (3.3 at%) MoS_2 nanosheets compared to the one of undoped MoS_2.

Stability is another momentous parameter to evaluate the performance of HER electrocatalysts. The chronopotentiometry technique was adopted to examine the overpotential stability with a fixed current density of 20 mA cm^{-2}. Stable overpotentials (135 mV, without *iR* corrections) with insignificant fluctuations are observed to maintain the current density of 20 mA cm^{-2} in acidic solutions over 10 h for the P-doped (3.3 at.%) MoS_2 nanosheets as illustrated in the inset of Figure 4d. After long-term durability tests, the P-doped MoS_2 nanosheets preserve their excellent activities with negligible loss of the current density, which further certifies their superior catalytic durability in acidic media. In general, the HER activity of MoS_2 nanosheets based on their exposed edges and catalytic sites would rapidly reach a limit owing to the poor interparticle (or interdomain) electron transport leading to insufficient conductivity.[9,12] Therefore, chemical doping is widely considered as an effective approach to improve the HER activity of the inert basal plane sites in MoS_2 as well as to increase the intrinsic electrical conductivity.[12,21,22] In this work, as demonstrated by XPS (Figure 3), the S constituents were partially replaced by P atoms in the MoS_2 crystal. Clearly, this substitution would induce more active unsaturated sites and defects in MoS_2 microstructures, resulting in a better catalytic performance for hydrogen generation. The increased activity may be related to the modified electronic structure of P-doped MoS_2. A smaller band gap was observed as compared with pristine MoS_2 after P doping, resulting in the lower adsorption free energy of hydrogen, as demonstrated in previous literatures.[22,23] However, with increasing P content, the electrocatalytic performance of MoS_2 nanosheets (e.g., 4.9 at.% P-doped sample with 90 min doping duration) becomes degraded, which may be contributed to the conducting behavior switch of MoS_2 by increasing the content of intercalated P in MoS_2, leading to a ruined conductance during the process of hydrogen generation. Also, at longer annealing times, restructuring of P-doped MoS_2 may further improve the crystallinity with less active site and defects. However, the detailed reason for the electrocatalytic performance degradation of highly doped (4.9 at%) P-MoS_2 is complex and requires more thorough studies in the near future. Nevertheless, all these findings have confirmed the favorable effect of P-doped MoS_2 nanosheets directly synthesized on carbon cloths as an attractive integrated electrode with the superior catalytic properties for hydrogen generation.

Conclusions

A facile post-growth phosphorus doping into MoS_2 nanosheets directly synthesized on carbon cloths was developed by utilizing low-temperature phosphidation. Phosphorus doping was found to change the surface chemical states of MoS_2 nanosheets, increasing their surface catalytic sites and facilitating better conductivity. The effects of different doping content and annealing durations were also investigated. Optimal phosphorus-doped (3.3 at.%) MoS_2 nanosheets exhibited substantially improved catalytic activity for the hydrogen evolution reaction with a low overpotential of 133 mV to drive the current density of 20 mA cm^{-2} and a small Tafel slope of 67.0 mV dec^{-1}, as compared with undoped MoS_2 nanosheets. All these results demonstrate the technological potency of our phosphidation approach to modify MoS_2 nanosheets to improve their catalytic properties for hydrogen generation.

Experimental Section

Nanosheet synthesis

Carbon cloths were washed with 10% HCl, ethanol and distilled water with ultrasonication sequentially, and then dried in air. MoS_2 nanosheets supported on carbon cloths (MoS_2/CC) were then prepared by using an as-reported hydrothermal method with some modification.[39] In detail, a piece of carbon cloth (1 by 3 cm) was immersed into 15 mL of transparent solution, containing 0.5 mmol of $Na_2MoO_4{\cdot}2H_2O$ and 1 mmol of $CS(NH_2)_2$. Next, the mixture was sealed in a Teflon-lined autoclave and heated at 373 K for 20 h. After cooling to room temperature, the obtained MoS_2 nanosheets supported on carbon cloths were washed with distilled water and ethanol alternatively for several times and then dried at 333 K overnight. By carefully measuring the mass of carbon cloth before and after synthesizing MoS_2, the loading mass density was calculated to be 2.8 mg cm^{-2}.

To prepare P-doped MoS_2 nanosheets, a low-temperature phosphidation method using $NaH_2PO_2{\cdot}H_2O$ as the phosphorous source was performed. Typically, $NaH_2PO_2{\cdot}H_2O$ (300 mg) and the obtained MoS_2/CC sample were placed upstream and downstream of a quartz furnace tube, respectively. The sample was then annealed at 673 K for 60 minutes with a temperature ramping of 10 K min^{-1} under the Argon (Ar) flow of 100 cm^3 min^{-1}. After cooling to room temperature with the continuous Ar purge, the P-doped MoS_2/CC catalysts were obtained. To study the effect of different annealing times on the catalytic property, the as-synthesized MoS_2 was treated under the identical process conditions for 30 and 90 min, respectively.

Materials characterization

Surface morphologies of the obtained samples were examined by using a scanning electron microscope (SEM, FEI Company, Oregon, USA/Philips XL30, Philips Electronics, Amsterdam, Netherlands). Crystal structures were determined by collecting XRD patterns on a Philips powder diffractometer using $Cu_{K\alpha}$ radiation ($\lambda = 1.5406$ Å) and imaging with a HRTEM (JEOL 2100F, JEOL Co., Ltd., Tokyo, Japan). Elemental mappings were then performed by using an EDS detector attached to a JEOL 2100F, and the chemical composition of the samples was measured. The chemical state of the as-prepared MoS_2 and P-doped MoS_2 nanosheets were examined by X-ray photoelectron spectroscopy (XPS, ULVAC-PHI5802). For the TEM studies, the nanosheets were first suspended in ethanol solution by ultrasonication and then drop-casted onto the grid for the subsequent characterization.

Electrochemical measurement

All the electrochemical tests were performed on a Gamry G300 electrochemical workstation (Gamry Instruments, USA). A setup of three-electrode system was employed to measure the electrochemical activity and stability of P-doped MoS_2/CC, in which the electrocatalysts, saturated calomel electrode (SCE), and Ti plate functioned as working electrode, reference electrode, and counter electrode, respectively. The geometrical active area of P-doped MoS_2/CC was defined by the silicon rubber for immersing into electrolytes. Linear sweeping voltammetry (LSV) curves were measured with a scan rate of 5 mV s^{-1} in 0.5 M H_2SO_4 solution (pH 0.6) for HER at room temperature. The HER stability tests were also performed by using chronopotentiometry in the basic solution. The potential scale with respect to reverse hydrogen electrode (RHE) was corrected by the Nernst equation, in which $E_{vs\ RHE} = E_{vs\ SCE} + 0.0592 \times pH + 0.242$ V. The *iR* corrections in polarization curves were performed using the current interrupt method provided by the Gamry G300 workstation.

Acknowledgements

We acknowledge the Science Technology and Innovation Committee of Shenzhen Municipality (Grants JCYJ20170307093131123 and JCYJ20160229165240684), "Qilu young scholar" program of Shandong University. We also acknowledge the General Research Fund of the Research Grants Council of Hong Kong SAR, China, under project number CityU 11275916, the National Natural Science Foundation of China (Grants 11404162, 51672229 and 61504151), the CAS-CSIRO project of the Bureau of International Co-operation of Chinese Academy of Sciences (122111KYSB20150064).

Conflict of interest

The authors declare no conflict of interest.

Keywords: doping · electrochemistry · hydrogen · molybdenum · phosphorous

[1] V. R. Stamenkovic, D. Strmcnik, P. P. Lopes, N. M. Markovic, *Nat. Mater.* **2017**, *16*, 57 – 69.
[2] S. Chu, Y. Cui, N. Liu, *Nat. Mater.* **2017**, *16*, 16 – 22.
[3] P. C. Vesborg, B. Seger, I. Chorkendorff, *J. Phys. Chem. Lett.* **2015**, *6*, 951 – 957.
[4] C. G. Morales-Guio, L.-A. Stern, X. Hu, *Chem. Soc. Rev.* **2014**, *43*, 6555 – 6569.
[5] Y. Zheng, Y. Jiao, M. Jaroniec, S. Z. Qiao, *Angew. Chem. Int. Ed.* **2015**, *54*, 52 – 65; *Angew. Chem.* **2015**, *127*, 52 – 66.
[6] J. R. McKone, S. C. Marinescu, B. S. Brunschwig, J. R. Winkler, H. B. Gray, *Chem. Sci.* **2014**, *5*, 865 – 878.
[7] D. Kong, J. J. Cha, H. Wang, H. R. Lee, Y. Cui, *Energy Environ. Sci.* **2013**, *6*, 3553 – 3558.
[8] H. Vrubel, T. Moehl, M. Grätzel, X. Hu, *Chem. Commun.* **2013**, *49*, 8985 – 8987.
[9] Y. Yan, B. Xia, Z. Xu, X. Wang, *ACS Catal.* **2014**, *4*, 1693 – 1705.

[10] L. Cheng, W. Huang, Q. Gong, C. Liu, Z. Liu, Y. Li, H. Dai, *Angew. Chem. Int. Ed.* **2014**, *53*, 7860 – 7863; *Angew. Chem.* **2014**, *126*, 7994 – 7997.
[11] B. Hinnemann, P. G. Moses, J. Bonde, K. P. Jørgensen, J. H. Nielsen, S. Horch, I. Chorkendorff, J. K. Nørskov, *J. Am. Chem. Soc.* **2005**, *127*, 5308 – 5309.
[12] W. Xiao, P. Liu, J. Zhang, W. Song, Y. P. Feng, D. Gao, J. Ding, *Adv. Energy Mater.* **2017**, *7*, 1602086.
[13] J. Xie, J. Zhang, S. Li, F. Grote, X. Zhang, H. Zhang, R. Wang, Y. Lei, B. Pan, Y. Xie, *J. Am. Chem. Soc.* **2013**, *135*, 17881 – 17888.
[14] J. Xie, Y. Xie, *ChemCatChem* **2015**, *7*, 2568 – 2580.
[15] D. Merki, H. Vrubel, L. Rovelli, S. Fierro, X. Hu, *Chem. Sci.* **2012**, *3*, 2515 – 2525.
[16] D. Escalera-López, Y. Niu, J. Yin, K. Cooke, N. V. Rees, R. E. Palmer, *ACS Catal.* **2016**, *6*, 6008 – 6017.
[17] J. Zhang, T. Wang, P. Liu, S. Liu, R. Dong, X. Zhuang, M. Chen, X. Feng, *Energy Environ. Sci.* **2016**, *9*, 2789 – 2793.
[18] D. Wang, D. Astruc, *Chem. Soc. Rev.* **2017**, *46*, 816 – 854.
[19] Y. Shi, B. Zhang, *Chem. Soc. Rev.* **2016**, *45*, 1529 – 1541.
[20] S. Anantharaj, S. R. Ede, K. Sakthikumar, K. Karthick, S. Mishra, S. Kundu, *ACS Catal.* **2016**, *6*, 8069 – 8097.
[21] X. Ren, Q. Ma, H. Fan, L. Pang, Y. Zhang, Y. Yao, X. Ren, S. F. Liu, *Chem. Commun.* **2015**, *51*, 15997 – 16000.
[22] P. Liu, J. Zhu, J. Zhang, P. Xi, K. Tao, D. Gao, D. Xue, *ACS Energy Lett.* **2017**, *2*, 745 – 752.
[23] R. Ye, P. del Angel-Vicente, Y. Liu, M. J. Arellano-Jimenez, Z. Peng, T. Wang, Y. Li, B. I. Yakobson, S. H. Wei, M. J. Yacaman, *Adv. Mater.* **2016**, *28*, 1427 – 1432.
[24] Q. Liu, X. Li, Q. He, A. Khalil, D. Liu, T. Xiang, X. Wu, L. Song, *Small* **2015**, *11*, 5556 – 5564.
[25] C. Wang, W. Wan, Y. Huang, J. Chen, H. H. Zhou, X. X. Zhang, *Nanoscale* **2014**, *6*, 5351 – 5358.
[26] C. Wu, Q. Fang, Q. Liu, D. Liu, C. Wang, T. Xiang, A. Khalil, S. Chen, L. Song, *Inorg. Chem. Front.* **2017**, *4*, 663 – 667.
[27] J. Zhang, T. Wang, D. Pohl, B. Rellinghaus, R. Dong, S. Liu, X. Zhuang, X. Feng, *Angew. Chem. Int. Ed.* **2016**, *55*, 6702 – 6707; *Angew. Chem.* **2016**, *128*, 6814 – 6819.
[28] Z. Pu, S. Wei, Z. Chen, S. Mu, *RSC Adv.* **2016**, *6*, 11077 – 11080.
[29] J. Kibsgaard, T. F. Jaramillo, *Angew. Chem. Int. Ed.* **2014**, *53*, 14433 – 14437; *Angew. Chem.* **2014**, *126*, 14661 – 14665.
[30] P. Xiao, M. A. Sk, L. Thia, X. Ge, R. J. Lim, J.-Y. Wang, K. H. Lim, X. Wang, *Energy Environ. Sci.* **2014**, *7*, 2624 – 2629.
[31] Z. Xiang, Z. Zhang, X. Xu, Q. Zhang, C. Yuan, *Carbon* **2016**, *98*, 84 – 89.
[32] A. Ambrosi, Z. Sofer, M. Pumera, *Chem. Commun.* **2015**, *51*, 8450 – 8453.
[33] D. Voiry, M. Salehi, R. Silva, T. Fujita, M. Chen, T. Asefa, V. B. Shenoy, G. Eda, M. Chhowalla, *Nano Lett.* **2013**, *13*, 6222 – 6227.
[34] X. Zou, Y. Zhang, *Chem. Soc. Rev.* **2015**, *44*, 5148 – 5180.
[35] X. Dai, K. Du, Z. Li, M. Liu, Y. Ma, H. Sun, X. Zhang, Y. Yang, *ACS Appl. Mater. Interfaces* **2015**, *7*, 27242.
[36] F. Lai, Y.-E. Miao, Y. Huang, Y. Zhang, T. Liu, *ACS Appl. Mater. Interfaces* **2016**, *8*, 3558 – 3566.
[37] F. Li, L. Zhang, J. Li, X. Lin, X. Li, Y. Fang, J. Huang, W. Li, M. Tian, J. Jin, R. Li, *J. Power Sources* **2015**, *292*, 15 – 22.
[38] C. C. L. McCrory, S. Jung, J. C. Peters, T. F. Jaramillo, *J. Am. Chem. Soc.* **2013**, *135*, 16977 – 16987.
[39] D. Hou, W. Zhou, X. Liu, K. Zhou, J. Xie, G. Li, S. Chen, *Electrochim. Acta* **2015**, *166*, 26 – 31.

Manuscript received: October 22, 2017
Revised manuscript received: November 24, 2017
Accepted manuscript online: November 30, 2017
Version of record online: February 6, 2018